


Article

Evaluation of Effective Elastic Properties for Wood–Cement Composites: Experimental and Computational Investigations

Jean Gérard Ndong Engone ¹, Ahmed El Moumen ², Chafika Djelal ¹, Abdellatif Imad ², Toufik Kanit ² and Jonathan Page ^{1,*} 

¹ Univ. Artois, IMT Nord Europe, Junia, Univ. Lille, ULR 4515, Laboratoire de Génie Civil et Géo-Environnement (LGCgE), F-62400 Béthune, France; jean.ndongengone@univ-artois.fr (J.G.N.E.); chafika.dantec@univ-artois.fr (C.D.)

² Univ. Lille, ULR 7512, Unité de Mécanique de Lille Joseph Boussinesq (UML), F-59000 Lille, France; ahmed.el_moumen@ensta-bretagne.fr (A.E.M.); abdellatif.imad@polytech-lille.fr (A.I.); tkanit@univ-lille.fr (T.K.)

* Correspondence: jonathan.page@univ-artois.fr; Tel.: +33-3-21-63-23-00

Abstract: In this work, wood–cement composites (WCC) based on poplar sawdust were developed and fabricated by the extrusion process. The volume fraction of wood particles in the mixes was varied from 23% to 46%. The mechanical properties of these WCC were characterized in compression to determine the maximum compressive strength and the Young’s modulus. In the second part, these Young’s modulus values were estimated in compression using a 3D numerical homogenization which takes into account the variability in wood particle lengths and the random distribution in the mixes. The obtained results show a good agreement between the experimental data and numerical calculations up to a 35% volume fraction. The model’s poor estimation for large volume fractions (over 35%) could be attributed to the experimental sample size, which is not representative for large volume fractions, the percolation of the wood particles into the mixes and the inhibition of the cement setting.

Keywords: wood–cement composites; effective elastic properties; numerical homogenization; mechanical properties



Citation: Ndong Engone, J.G.; El Moumen, A.; Djelal, C.; Imad, A.; Kanit, T.; Page, J. Evaluation of Effective Elastic Properties for Wood–Cement Composites: Experimental and Computational Investigations. *Sustainability* **2022**, *14*, 8638. <https://doi.org/10.3390/su14148638>

Academic Editor: Nassim Sebaibi

Received: 20 May 2022

Accepted: 11 July 2022

Published: 14 July 2022

Publisher’s Note: MDPI stays neutral with regard to jurisdictional claims in published maps and institutional affiliations.



Copyright: © 2022 by the authors. Licensee MDPI, Basel, Switzerland. This article is an open access article distributed under the terms and conditions of the Creative Commons Attribution (CC BY) license (<https://creativecommons.org/licenses/by/4.0/>).

1. Introduction

Over the past several years, environmental-protection objectives have led the construction industry to produce sustainable building techniques with the use of bio-based materials. Likewise, much research has been conducted to introduce plant fibers in cementitious materials [1–4]. A wide array of plant fibers are available for manufacturing plant-fibers-based cementitious composites, with various dimensions and shapes [5]. In the literature, plant fibers stemming from coconut [6,7], sisal [8,9], eucalyptus [10], bamboo [11], rice husk [12], malva [13], hemp [14], wood byproducts [15], palm [16], bagasse [17] and flax [18] are often included in the form of short or long fibers to produce cement composites. These vegetal particles contain significant amounts of cellulose, hemicelluloses, and lignin [19]. Moreover, their incorporation into a cementitious material has an impact on chemical reactions. Thereby, they influence the hardening of such materials by inhibiting these reactions [20–22], resulting in a reduced formation of hydrated calcium silicates (CSH) and lower composite compressive strengths. On the other hand, these plant-based reinforcements often substantially improve the flexural strength, toughness [23] and impact resistance of the composite [24]. These materials may also offer other advantages, such as good thermal [25], acoustic [26] and fire-resistance properties [27], depending on the plant fiber and the composite-mix design. Indeed, lower composite density and the composite’s low cost enables a reduction in both the weight and cost of the designed material [28].

However, over time, the efficiency of plant-based reinforcements may decrease due to both the aggression of chemical (alkaline) components in the cement matrix and to the mineralization of plant particles by the hydration products' migration through component pores [29]. In addition, the hydrophilic nature of these materials makes them sensitive to size variations over a wide range of heat settings. This dimensional instability impairs the mechanical properties of cement composites [30]. To overcome these issues, many studies have been conducted to find new processes with an improvement in or stabilization of the composite properties [31]. It should be noted that substituting cement with silica fumes [32] has enhanced cement composite durability. Silica fumes react with the calcium hydroxide located at the cement matrix/plant fiber interface to form additional hydrated calcium silicates (CSH) [33]. This phenomenon raises the level of adherence between the cementitious matrix and the reinforcements, while minimizing the dimensional variations in reinforcements.

In recent years, numerous studies have dealt with the use of wood byproducts such as sawdust [34–36], wood chips [37,38], wood fibers [21] and wood ash [39,40] for incorporation into wood–cement composites (WCC). For valorization, byproducts come from both hardwood [41,42] and softwood species [21,43,44]. Despite this numerous research devoted to wood-based composites, their use in the field of construction remains marginal, and is mainly devoted to partitioning walls and acoustic and/or thermal insulation. The weak mechanical properties generally observed on these composites, as well as their limited or unknown durability, can explain the low use of these wood composites in construction. In addition, the variability in such characteristics with respect to both manufacturing conditions and the materials employed influence composite use. Therefore, predicting composites' mechanical behavior becomes essential. Usually, a mechanical-behavior prediction for WCC is based on statistical studies of experimental results [38]. Note the few numbers of studies actually dedicated to predicting the mechanical behavior of wood–cement composites using numerical modeling. The understanding of the mechanical and structural behavior of WCC could contribute to improving and designing its properties at the minimum cost [45].

This study aims to evaluate the possibility of using existing mechanical numeric models for mortars and concretes, on wood-based cementitious composites, to identify the limits and the parameters that must be adapted in these models. This work is based on a joint comparison of numerical modeling and experimental results. Therefore, a prediction of the mechanical behavior of WCC based on elastic behavior (calculation of Young's modulus) is proposed. This prediction is carried out by comparing three approaches: an experimental approach, an approach based on common homogenization techniques and a 3D numerical-modeling approach. An experimental program was also performed for manufacturing a wood-based composite based on a cementitious binder and wood sawdust by an extrusion process. Indeed, sawdust particles were introduced into the mixture by replacing the sand. The volume content of wood particles into the different investigated mixes varies from 23% to 46%. The Young's modulus of these composites was measured experimentally through uniaxial mechanical testing in compression. Thereafter, these compression Young's modulus were estimated using a numerical-homogenization technique, based on a 3D numerical-homogenization approach. For this modeling, we used the finite element method, while the theory of bounds was chosen to perform the analytical approach. The geometric 3D modeling also considered the variability in wood particle lengths with a random distribution. The experimental and numerical data were compared in order to validate the numerical homogenization approach.

2. Experimental Program

2.1. Materials

This work aims to develop a wood-particle (WP)-reinforced cementitious composite derived from wood waste (from sawmill). The wood particles used in this study originate from poplar, which is a hardwood grown extensively in the northern France. The morphologies at various scales of these WP are of a random shape (Figure 1a). A 2D image analysis provided different dimensions (Figure 1b).

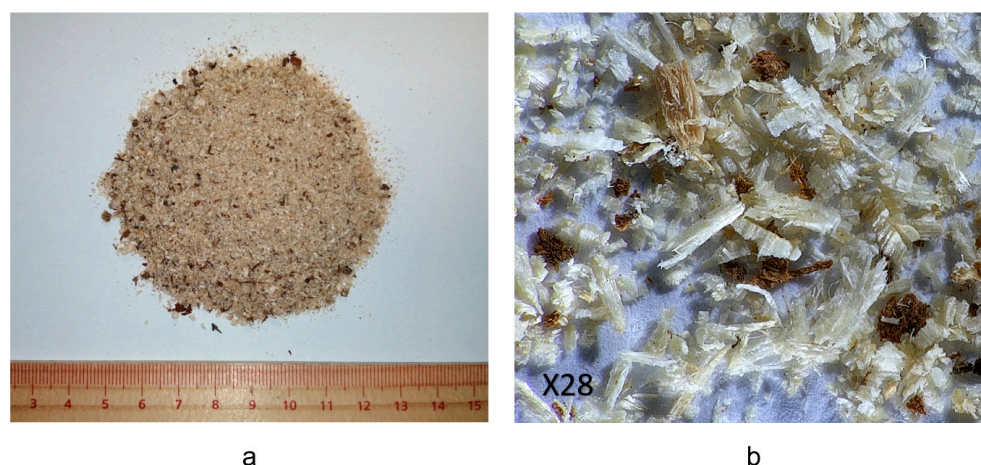


Figure 1. (a) wood particles (WP) observation with the naked eye, (b) microscopic observation of wood particles.

The average maximum and minimum lengths are, respectively, 25 mm and 80 μm , while the average maximum and minimum widths were recorded as 4.4 mm and 80 μm , respectively. The largest sized aggregates are of 2%, which matches the proportion of minimum-sized aggregates.

The apparent and real densities of wood particles are 0.178 and 0.390 g/cm^3 , respectively. Wood is known for its high water sensitivity, characterized by a large water-absorption capacity, often exceeding twice its own weight. This water sensitivity could significantly affect the material properties in fresh and hardened states [20]. The water absorption kinetics was also assessed, providing information on the water absorption rate of the WP and the time until saturation, which is 2 min for these wood particles. During specimen production, this time will be respected for WP water saturation. The water absorption capacity after 24 h is 174%.

The sand used in this study comes from the Seine river with a 0/4 particle grading, a coefficient of absorption of 0.49% and a real density of 2.61 g/cm^3 . The cement used for the composite manufacturing is a CEM I 52.5 N, with a real density of 3.11 g/cm^3 and a 98% clinker content.

2.2. Mix Design and Extrusion of Wood–Cement Composites (WCC)

The objective of the extrusion process performed herein was WCC-block manufacturing with these dimensions: 105 mm \times 60 mm \times 220 mm, in accordance with to the NF EN 771-1/CN French standard. Extrusion is an efficient manufacturing process consisting of forcing the flow of a plastic material or a fluid product through a die whose dimensions have been defined beforehand and depend on the intended use of the extruded product. In this work, 7 mixes were designed and extruded (Table 1). One design composed solely of sand, cement and water was optimized for this extrusion process and then set as the reference design (WCC₀).

Table 1. Various constituents concentrations of wood mortars, with $\delta_{(C+W)}$, $\delta_{(S)}$ and $\delta_{(WP)}$ being volume ratio of paste (cement + water), sand and sawdust in the mixture, respectively.

Mix Design	Volume Ratio			Concentrations (kg/m ³)			
	$\delta_{(C+W)}$	$\delta_{(S)}$	$\delta_{(WP)}$	Cement	Water	Sand	Wood Particles
WCC ₀	40%	60%	0%	488	244	1568	0
WCC ₂₃	40%	37%	23%	646	194	985	91
WCC ₂₆	40%	34%	26%	646	194	806	114
WCC ₃₂	40%	28%	32%	646	194	730	125
WCC ₃₅	40%	25%	35%	646	194	653	137
WCC ₄₀	40%	20%	40%	646	194	501	159
WCC ₄₆	40%	14%	46%	646	194	348	182

The sand was partially substituted (in volume) in this composition by WP in the mix, varying from 23% (WCC₂₃) to 46% (WCC₄₆) (Table 1). However, the cement paste content was set to 40% in volume and the water-to-cement ratio to 0.3, in all mixes. Moreover, in order to avoid the absorption of the effective water used for the cement matrix hydration, the wood particles were saturated for 2 min prior to mixing process. Then, the sand and the cement were added into the mixture, and mixed for 1 min before introducing the water progressively for 1 min. Then, a 3-min mixing cycle was run to homogenize the mixture. The WCC₀ mortar formulation was optimized for extrusion by varying the cement paste volume (cement + water) and water–cement ratio to obtain an extrudable mix. These choices of wood-particle incorporation ratio were derived from a previous study conducted on the optimization of mortar extrusion using wood sawdust for masonry building block [46]. The greater quantity of paste volume generates the reduction in inside mix friction and of friction between extruder-wall and mix. Any rheology modifiers or similar chemical admixtures were used to avoid complex physicochemical interactions in the mix. Indeed, interactions between wood particles and rheology modifiers or chemical additions are not well-studied in the literature.

The extrusion step was carried out with a piston extruder [47], with a 5 mm/s extrusion speed. Following extrusion, the resulting blocks were stored in a humidity-controlled room at a temperature of 20 ± 2 °C and a relative humidity of $65 \pm 5\%$, until physical or mechanical tests.

The mass density of the hardened specimens was determined at 14 days, according to EN 12390-7 standard. Figure 2 displays the mass density evolution according to the wood-particle content into the different mixes. A decrease in the mass density can be noted as the wood particle volume in the mix increases. Compared to the reference composite (WCC₀), wood particles lead to a relative drop in density from 19% (with WCC₂₃) to 35% (with WCC₄₆). A polynomial regression type confirmed by a very good correlation coefficient (0.99) was obtained. This drop may be correlated with the mass density difference between sand and WP. It turns out that the density of sand (equal to 2.64 g/cm³) is eight times higher than that of WP (equal to 0.39 g/cm³). The low density inherent in extruded blocks constitutes a real advantage in terms of reducing structural weight.

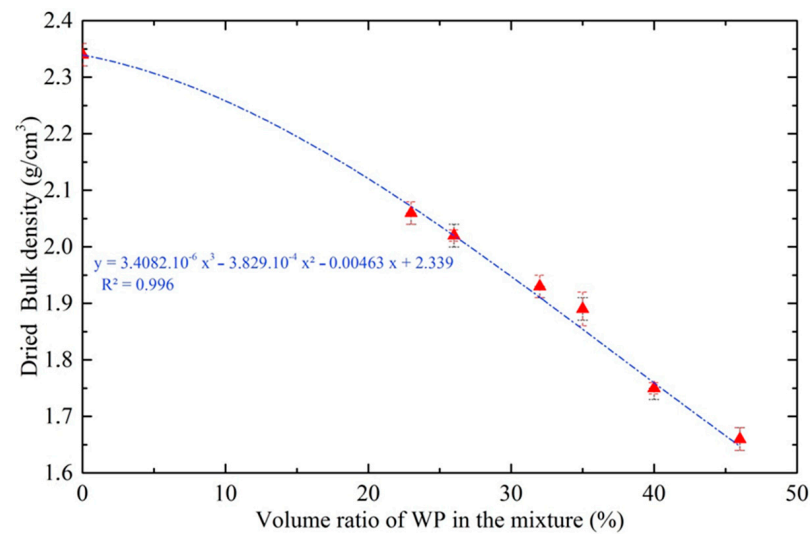


Figure 2. Dry density of WCC specimens versus volume ratio of wood particles, at 14 days.

2.3. Mechanical Tests

The compression test was performed in accordance with the EN 772-1 standard, using a loading speed of 7 kN/s. Three specimens were tested for each test. Both stress and strain were recorded during the test.

In Figure 3 are presented typical compressive stress–strain curves for three mixes (WCC₀, WCC₂₃ and WCC₃₅). The increase in the volume ratio of WP leads to a reduction in the Young’s modulus and the maximum strength. An increase in strain at the failure point is also noted. The incorporation of wood particles into the mixes seems to improve the composites strain. This phenomenon is due to the high deformability of wood particles, which allows composites to deform significantly under low stress.

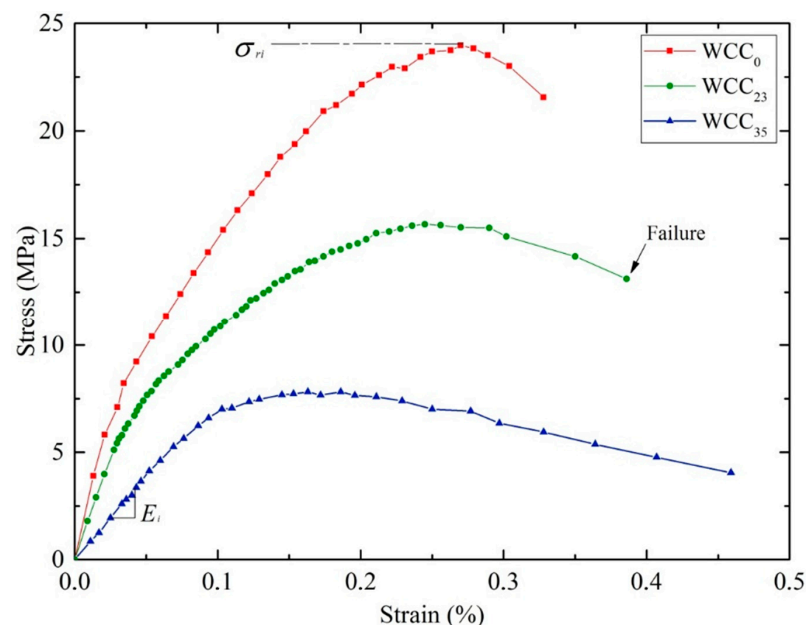


Figure 3. Example of stress–strain curves obtained during the compressive test, at 14 days.

The average Young’s modulus (E_m) was determined from the stress–strain curves. In Figure 4 is shown the Young’s modulus according to the wood volume in the composite after 14 days of curing. The Young’s modulus decreases as wood volume in the mix increases. Similar results were obtained by Bashar et al. for wood-chip-based composites [37].

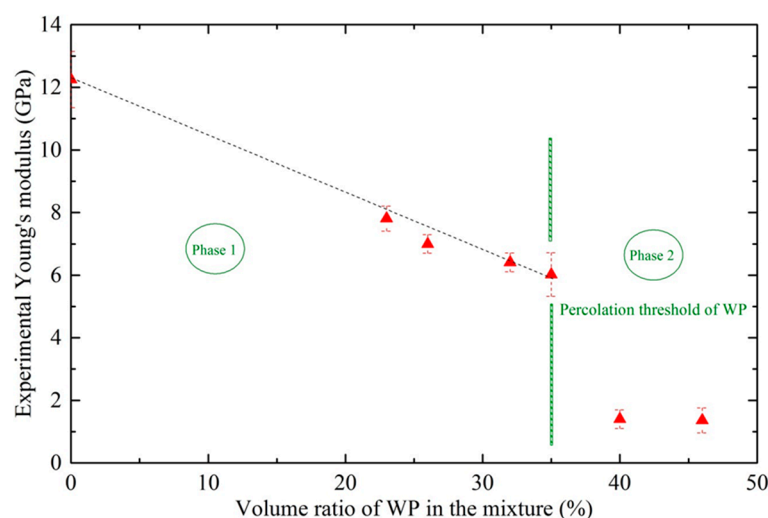


Figure 4. Young modulus of WCC specimens versus volume ratio of WP after 14 days.

Two different zones can be distinguished in Figure 4. In the first area, a linear decline of the Young's modulus is observed, up to 35% of wood particles. For this WP content, the Young's modulus is 6.02 GPa, corresponding to a relative reduction by 51%. This decrease in the Young's modulus in the first area can be attributed to various parameters, including the inhibition of the cement hydration reaction, the increased mixture porosity, the low stiffness of wood particles (WP), and the distribution of the WP in the mixture [46]. The perturbation or inhibition of the cement hydration occurs in the fresh state during the contact between cement paste and wood particles. The alkaline matrix derived from the cement dissolution interact with the polysaccharides present in wood particles. This chemical interaction either disturbs or inhibits the cement hydration, which is the primary parameter controlling the microstructure formation and responsible for cementitious-material mechanical properties [21,48,49]. The assessment of the influence of the wood particles used in this study on the cement hydration (in a standardized mortar) has been demonstrated on previous studies using an isothermal calorimeter with a temperature setting of 20 °C [46]. The same experimental procedure was performed on three mixes (WCC₀, WCC₃₅ and WCC₄₆). In Figure 5 is presented the heat flow evolution (in isothermal conditions) of the fresh mixes during the 48 h after mixing. It can be observed that the incorporation of wood particles leads to a reduction in the maximum heat flow peak. This is accompanied by a slowdown of the kinetics of hydration. Thus, the introduction of wood particles disturbs the cement hydration of the fresh composite, which may affect the formation of cement hydrates. In parallel, there is a delay in the appearance of the maximum heat peak, which suggests that the cement hydration in the mix is gradually disturbed. The maximum heat flow reductions are by 26% and 39% for WCC₃₅ and WCC₄₆, respectively. The time of the cement setting is 2 h 30 min for the WCC₀ and more than 5 h for WCC₃₅ and WCC₄₆ composites. The setting time delay is, therefore, approximately equal to 2 h 30 min, i.e., a doubled setting time. This inhibition is even more pronounced as the content of wood particles in the composite is high.

The porous structure of wood particles leads to an increasing in the composite porosity [46]. During the compressive tests, this porosity leads to a reduction in the compactness of the composite, which would reduce the mechanical performance. The random distribution of wood particles and their elongation will create weakness areas in the composite structure. This effect on the composite mechanical behavior is related to the wood-particle content in the composite.

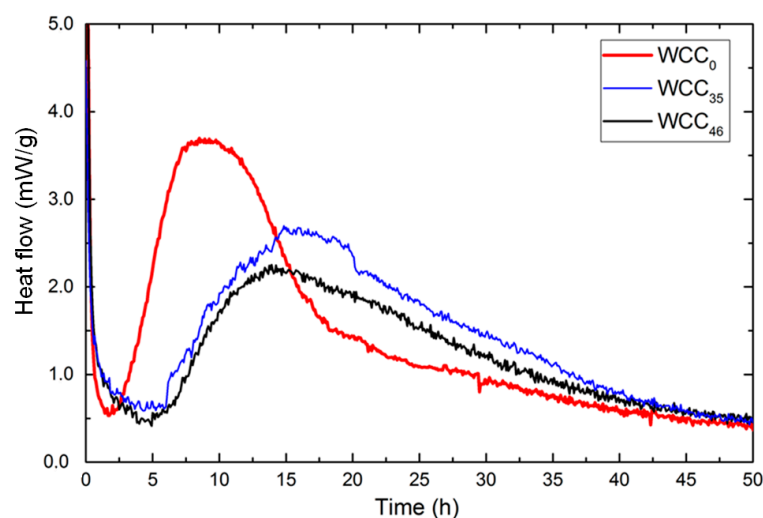


Figure 5. Typical hydration isotherms (heat flow vs time) for three mixes.

Beyond a wood-particle volume content of 35%, a strong decrease in the Young's modulus is noticed, with a lower value of 1.40 GPa, i.e., a relative decrease by 89% in comparison with WCC_0 . This wood-particle (WP) content seems to correspond to a threshold volume beyond which WP percolates into the composite. Several micrographs were performed on several longitudinal sections and cross-sections of the blocks in a previous study [36]. The observations confirmed the assumption of WP percolation. Saturation can be observed in the structure by wood particles from the WCC_{40} compared to other composites.

The saturation of wood particles leads to a percolation phenomenon, which modifies the composite mechanical behavior [47]. Due to this percolation, the wood particles are randomly entangled, which leads to a higher composite porosity and creates a large area of minimum stiffness. This increased porosity may also be linked to the high water-absorption capacity of the aggregates, causing dimensional variations in the plant particles. The higher porosity of extruded mortars incorporating wood particles was also highlighted in a previous study [36]. The mechanical strengths will then be deteriorated due to this greater porosity. Furthermore, due to the flexibility of the wood particles, this also creates zones of weakness in the composite, which tend to reduce the rigidity of the block (reduction in the Young's modulus), and, therefore, of the mechanical properties.

In addition to the effect of the WP percolation, the chemical interactions between wood and cement may also significantly influence the mechanical properties and then decrease the Young's modulus. The extent of setting inhibition is, in fact, proportional to WP volume in the mix, as the wood volume fraction increases the quantity of inhibiting agents [46]. The decrease in a composite's mechanical properties could be associated with a percolation phenomena coupled with inhibition.

The normalized Young's modulus of the composites was calculated from Equation (1). This equation is widespread in the literature [50].

$$\frac{E_c}{E_0} = C \cdot \left(\frac{\rho_c}{\rho_0} \right)^n \quad (1)$$

In the previous equation, the subscript E_0 , ρ_0 and E_c , ρ_c denote the Young's modulus and the bulk density of the reference mix and the composite, respectively. C and n are constants determined by experiments.

Considering the experimental results for WCC_0 to WCC_{35} , a relative function of the Young's modulus was obtained with Equation (2).

$$\frac{E_c}{E_0} = \left(\frac{\rho_c}{\rho_0} \right)^{3.4} \quad (2)$$

Normalized Young's modulus and the relative function expressed by Equation (2) (relative modulus of elasticity) are expressed according to the normalized density in Figure 6. In phase 1, there is a good correlation between the relative function and the normalized Young's modulus. In phase 2, the values of the relative function are greater than the normalized Young's modulus. This can be explained by the percolation phenomena and the significant inhibition of cement hydration, which does not allow good agreement with the normalized Young's modulus.

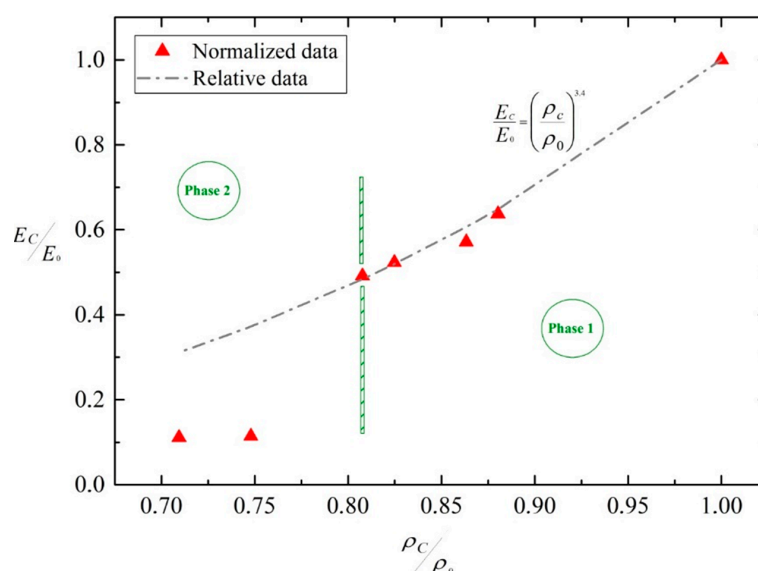


Figure 6. Normalized Young's modulus according to the normalized bulk density.

3. Predictive Numerical Modeling

The experimental characterization of cement–wood composite specimens was presented in the previous section. In keeping with the experimental characterization, this section aims to numerically simulate these material properties. The macroscopic elastic behavior of the material was studied using a multi-scale analysis, based on knowledge of the mechanical behavior of each phase of the composite. For this multi-scale analysis, numerical techniques based on the finite element method (FEM) as well as analytical homogenization models were used. Following this, a comparison between the results of the homogenization steps (analytical and numerical) and the experimental results was, finally, proposed.

There are several analytical methods that can be used to evaluate the effective elastic properties of multiphase composites. The most common are the Voigt and Reuss (VR) bounds [51,52], Hashin and Shtrikman's bounds (Hashin and Shtrikman [53]) and Mori-Tanaka's theory [54]. The proposed estimation typically depends on inclusion parameters, such as the particle shape and its distribution. These models converge whenever the volume fraction of particles (inclusion) or the difference between the properties of both phases is insufficient. Otherwise, a notable difference and divergence becomes apparent. However, in this study, a numerical method was used to solve the homogenization problems. In this case, it is essential to consider the concept of representative voluminal element (RVE). The RVE must contain a sufficiently large number of wood particles as in cementitious materials, while remaining small enough to both allow the convergence and to be considered as a volume element of continuum mechanics [55].

Several methods numerically generate the geometry of cement composites. Some methods are based on a simple shape (sphere), such as those of Bentz [56], Béjaoui et al. [57] and Bishnoi et al. [58]. Nagai et al. assessed the linear elastic behavior of concrete using successive 2D sections to obtain the 3D concrete microstructure [59]. Wriggers et al. introduced a model of concrete made of spherical particles (concrete aggregates) associated to a

cement matrix [60]. In this model, the material is supposed to be isotropic and numerical outputs of the effective properties are obtained. Otherwise, Caballero et al. has proposed a model of concrete as aggregates generated in the form of polyhedra, as obtained by the Voronoï tessellation, into a mortar composite [61]. Recently, Escoda et al. developed model based on a random morphology for concrete microstructures using a multiscale Poisson polyhedral [62]. This two-phase model used cementitious matrix aggregates. He et al. tested both of the polyhedral and ellipsoidal shapes and compared with various models based on X-ray tomography data [63].

In this section, the mechanical properties of wood–cement composites will be determined with homogenization techniques and will be compared with experimental data presented in Section 2.2. In addition, this study proposes to investigate the accuracy of some analytical models widely used for cementitious materials by way of comparison with experimental data and numerical simulations. For this purpose, 3D cement-composite samples were generated in various volume fractions (0% to 46%).

3.1. Analytical Homogenization Models

In the literature, there are different methods of analytical homogenization, the most widespread of which are based on an approach in the isotropic case: the Voigt [51] and Reuss [52] first-order bounds (VR), the Mori and Tanaka (MT) model [54], and the Hashin and Shtrikman optimal bounds (HS) [53]. Elastic properties of composites can be determined from these models from the properties of each phase, “*m*: matrix” and “*i*: inclusion”, and wood volume fraction “*p*”. Analytical expressions are provided in Equations (3)–(9) and (12):

- VR bounds

$$E^{Voigt} = pE_i + (1 - p)E_m \quad (3)$$

$$E^{Reuss} = \frac{E_i E_m}{(1 - p)E_i + pE_m} \quad (4)$$

- Upper and lower HS bounds, HS^+ and HS^-

$$\begin{cases} k^{HS^-} = k_m + \frac{p}{1/(k_i - k_m) + 3(1-p)/(3k_m + 4\mu_m)} \\ k^{HS^+} = k_i + \frac{(1-p)}{1/(k_m - k_i) + 3p/(3k_i + 4\mu_i)} \end{cases} \quad (5)$$

$$\begin{cases} \mu^{HS^-} = \mu_m + \frac{p}{1/(\mu_i - \mu_m) + 6(1-p)(k_m + 2\mu_m)/5\mu_m(3k_m + 4\mu_m)} \\ \mu^{HS^+} = \mu_i + \frac{(1-p)}{1/(\mu_m - \mu_i) + 6p(k_i + 2\mu_i)/5\mu_i(3k_i + 4\mu_i)} \end{cases} \quad (6)$$

The bulk k and shear μ modulus were calculated with HS analytical models. To derive Young’s modulus E , Equation (5) allow relations all of elastic properties. Note that E^{HS^+} and E^{HS^-} represent upper and lower Young’s modulus, respectively.

$$E^{HS^\pm} = \frac{9k^{HS^\pm}\mu^{HS^\pm}}{(3k^{HS^\pm} + \mu^{HS^\pm})} \quad (7)$$

- Mori–Tanaka model

$$k^{MT} = k_m \left(1 + \frac{p(k_i - k_m)}{k_m + \alpha(1 - p)(k_i - k_m)} \right) \quad (8)$$

$$\mu^{MT} = \mu_m \left(1 + \frac{p(\mu_i - \mu_m)}{\mu_m + \beta(1 - p)(\mu_i - \mu_m)} \right) \quad (9)$$

$$\alpha = \frac{3k_m}{3k_m + 4\mu_m} \quad (10)$$

$$\beta = \frac{6(k_m + 2\mu_m)}{5(3k_m + 4\mu_m)} \quad (11)$$

Finally, from the Equation (12) is calculated the Mori–Tanaka Young’s modulus, E^{MT} .

$$E^{MT} = \frac{9k^{MT}\mu^{MT}}{(3k^{MT} + \mu^{MT})} \quad (12)$$

The evolution of the homogenized Young’s modulus according to the wood volume fractions was studied (Figure 4). For volume fractions ranging from 0% to 46%, the analytical results were plotted and compared with experimental data provided by the compression test on WCC specimens.

With proportions of wood particles up to 35%, the experimental Young’s modulus values of WCC are always close to the HS bounds, which is in agreement with homogenization theory (Figure 7). Furthermore, experimental results closely match with both MT models and HS bounds. Beyond a proportion of 35%, the experimental values are below the values of all investigated models, and even the VR model, which has the lowest modulus values. This limit is correlated to the percolation threshold, as highlighted in Figure 4. This difference also depends on the testing sample dimensions, which may no longer be representative for high WP volume fractions. It seems reasonable to question the effect of specimen size on the elastic properties for proportions varying from 40% to 50%. Moreover, the chemical interactions in the composites in a fresh state (significant inhibition of the cement and wood particles) could explain the poor model estimation for large volume fractions, which does not consider this interaction.

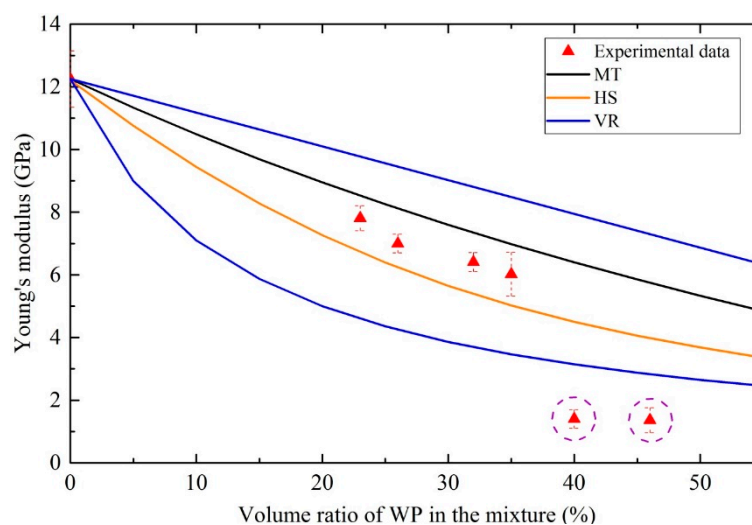


Figure 7. Homogenized Young’s modulus: experimental and analytical results.

3.2. Numerical Simulations

This part is devoted to the prediction of the effective properties on the representative volume element (RVE) using numerical methods. For that purpose, two-phase microstructures including a cementitious-matrix phase and a wood-particle phase with various volume fractions were generated. These microstructures will be introduced into the finite element model to compute the effective properties. Then, a comparison between numerical data, analytical modelling and experimental results is proposed.

3.2.1. Mesh of Microstructures

The numerical techniques for composite-material modelling are based on the conception of a representative microstructure. For the virtual microstructure to approximate the real one, the most common method consists of generating random microstructures taking into account experimental parameters such as particle shape, particles size, and particle distribution. Here, random microstructures were generated by the Poisson’s process, which

has already been implemented in several works to represent composite microstructures (El Moumen et al. [64] and El Moumen et al. [65] for the algorithm methodology).

Figure 8 presents some 3D representations of wood–cement-composite (WCC) microstructures derived by the Poisson process and then used for simulations. The image of the microstructure is associated with a regular finite element mesh by superposition, according to the multi-phase element method, developed by Lippmann et al. [66] and used to estimate the elastic properties of biocomposites. A microstructure image is introduced to attribute the phase properties of a regular mesh to each integration point, in accordance with the underlying voxel color. A random distribution of wood particles (WP) is also observed. A dense distribution of the WP is obtained from 40% of the volume fraction (Figure 8b). Figure 8d shows a section of the random microstructure of the WCC₄₀, a large proportion of WP are observed in the sample.

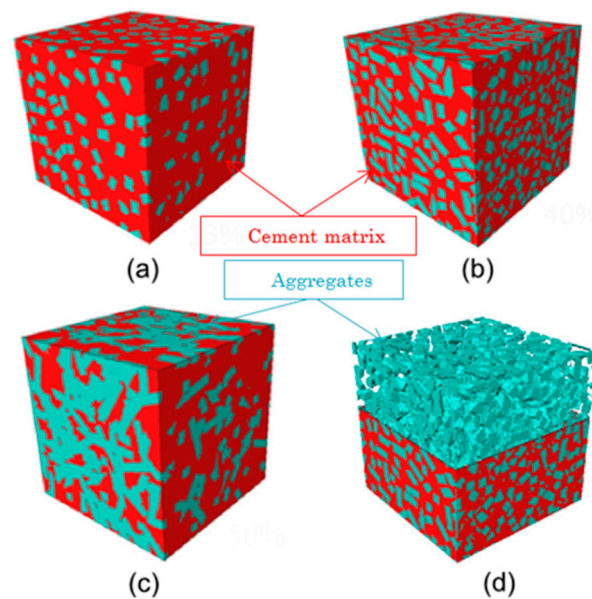


Figure 8. Representation of microstructures with different volume fractions of aggregates, (a–d) being the volume fractions of 23%, 40%, 50% and the inside cut of 40% volume fractions.

Figure 9 exhibits an example of the meshed microstructure. Concerning numerical simulations, the use of structured meshes was privileged since the free-mesh technique typically leads to an increase in the number of elements, and a more expensive computation. The considered elements are 20-node quadratic bricks with 27 integration points.

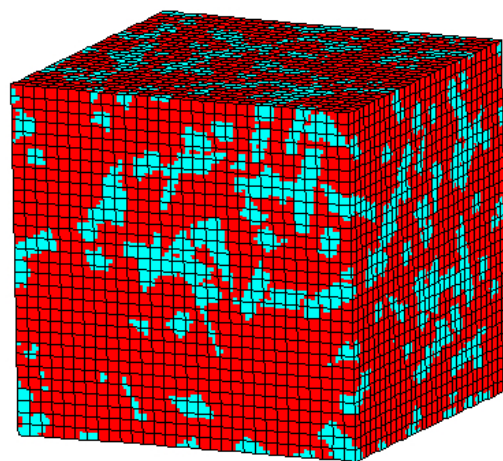


Figure 9. Mesh of microstructures used for numerical simulations.

3.2.2. Boundary Conditions and Mesh Density

For numerical simulations, the mechanical loading is applied to one face of the microstructure while the opposite face has no loading. Note that these loadings constitute the compression test implemented during the experimental approaches. As an illustration, the expression of these boundary conditions is given in Equation (13):

$$\begin{cases} \bar{u} \{face(x = 0, y, z) = 0\}; \bar{u} \{face(x = L, y, z) = d\} \\ \bar{v} \{face(x = 0, y, z) = 0\}; \bar{w} \{face(x = 0, y, z) = 0\} \end{cases} \quad (13)$$

where \bar{u} , \bar{v} and \bar{w} are the displacements applied in x , y and z directions, L is the length of the microstructure, and d is the displacement imposed in x direction.

The number of elements used to mesh the elementary cement–wood volume is defined as the mesh density. Therefore, a specific 3D microstructure composed of 200 random wood particles was considered. The number of particles and the microstructure geometry is fixed, even though various mesh resolutions were used. In Figure 10 is presented the variation in the homogenized Young's modulus for different numbers of elements. The number of nodes increases from 756 (for a 125-element mesh) to 116,281 (for a 27,000-element mesh) while maintaining the same volume composed of 200 particles occupying 23%.

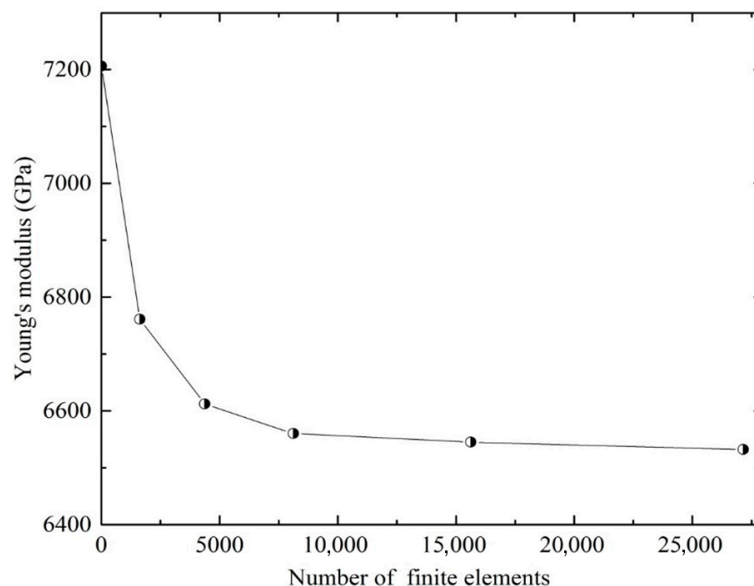


Figure 10. Variation in the homogenized Young's modulus for different number of FE.

The Young's modulus strongly decreases for the first meshes (with few elements); then, a stabilization is observed for the highest mesh density. In Figure 10 the number of finite elements where convergence begins can be observed, at approximately 8000 elements/200 particles. Due to convergence, a mesh density of 40-quadratic elements per particle seems to be necessary.

3.2.3. Estimation of the Effective Elastic Properties

A simple uniaxial compression test, adopting the defined boundary conditions, was applied to the WCC microstructure. The homogenized effective Young's modulus can then be determined. The numerical results obtained for the different particle volume fractions are shown in Figure 11, and compared with experimental results. As expected, the Young's modulus decreases when the WP volume content increase, which is in good agreement with the results obtained experimentally. However, a notable difference between the numerical and experimental results is observed in the case of a WP content greater than 35%. From this rate, the homogenization models and numerical modeling used do not make it possible to

correctly estimate the composite mechanical properties. In this study, low impact provides a good estimate of the elastic properties.

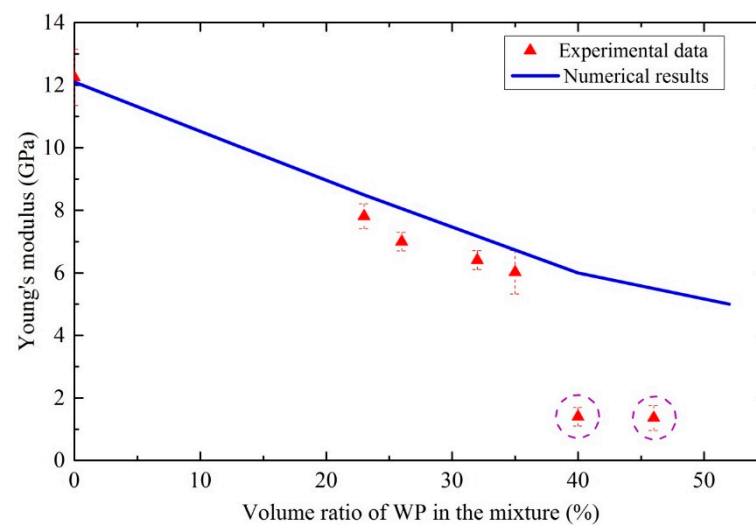


Figure 11. Homogenized Young's modulus according to the WP content: comparison between experimental and numerical results.

The numerical methods used in this work for estimating the effective properties are based on the micromechanics interaction between the composite constituents. In the present study, the composites are partially composed of wood particles (WP). It was noted previously that there was a chemical interaction between these particles and the cement, and even more for high WP content. Furthermore, a percolation effect of the wood particles, due to their high water absorption, was also highlighted. Thus, for low levels of incorporation of wood particles, these two phenomena, related to the particles, are not too significant on the elastic mechanical properties. Thus, in the case of our study, the models used make it possible to correctly estimate the mechanical properties of the composites, for WP rates below 40%.

For high wood-particle content, the effect of chemical interactions is more significant, which could explain the incorrect estimation of the effective properties with the numerical modelling. The mechanical characteristics of the matrix are different from those the reference matrix (with 0% WP). Homogenization models and numerical simulation does not take into account the change in the properties of the matrix due to chemical interactions between cement and wood. Otherwise, the percolation phenomenon observed in Figure 4 could also be responsible for poor estimation of the effective elastic properties. Homogenization theory assumes that the inclusion is perfectly coated with the matrix (as mineral aggregates). Due to WP percolation, this assumption cannot be respected, which could affect the bounds of homogenization.

The estimation of the effective properties is also strongly influenced by the representative volume element that allows consideration of each phase of the composite. The size of the experimental samples seems to not be sufficiently representative in the case of a large volume content.

As a means of illustration, the compression test was performed in linear elasticity, and the local Young's modulus at each point was plotted in a chart distribution (Figure 12). It seems that the local Young's modulus distribution between the two phases of the microstructure was altered after loading. It can also be deduced that the volume fraction and particle distribution are the geometric parameters most heavily influencing local WCC properties.

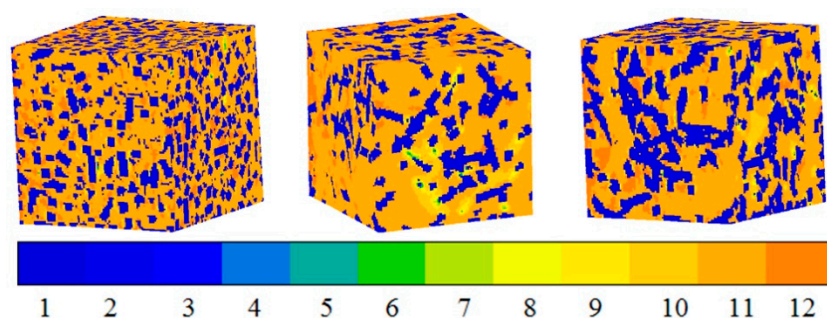


Figure 12. Local distribution of Young's modulus, in GPa, for different configurations.

4. Conclusions

In this study, compressive tests were performed to highlight the influence of wood particles (WP) on behavior in the compression of extruded wood–cement composites (WCC). The mechanical properties were experimentally determined. A predictive modeling of the mechanical properties of these composites was performed by using a numerical homogenization method. From this study, the following conclusions can be drawn:

- The Young's modulus of wood–cement composites decreases with the increase in WP content. Two behavioral phases can be observed. An almost linear drop in the normalized modulus of elasticity as a function of the WP rate, up to a rate of 35%. This volume corresponds to the percolation threshold of the wood particles in the mixture. From this level and extending to a volume of 46%, the loss of mechanical properties in compression is considerable. Above a 40% WP volume, the higher WP in WCC exerts a very low influence on the mechanical properties of composites.
- The estimation of the Young's modulus by homogenization analytical method shows that the Mori–Tanaka model (MT) and upper Hashin and Shtrikman bounds (HS) allow a good approximation of mechanical properties in the case of a low proportion of wood particles in the mixture. Beyond 35% WP volume, conventional homogenization models are not appropriate to approximate the mechanical properties. Indeed, the percolation of wood particles and cement hydration disturbances result in a poor assessment of the modulus of elasticity.
- The numerical homogenization procedure was performed using the finite elements method based on a representative volume element (RVE). The contrast between the numerical results and experimental approach allow a good approximation of mechanical properties up to a 35% threshold volume. Beyond the percolation threshold, the numerical microstructure does not match the actual microstructure. In addition, the inhibition of the cement hydration may be greater. However, this poor estimation can also depend on the experimental sample size, which is no longer representative for large volume fractions. It seems legitimate to question the effect of specimen size on the elastic properties for proportions varying from 40% to 50%.

The next phase of this work will take into account the actual microstructure of composites by performing a tomographic study. The effect of inhibition will also be taken into account by performing a post-treatment of the wood particles. In addition, a study of the representative volume element will be performed.

Author Contributions: Conceptualization, J.G.N.E., C.D., A.I. and J.P.; methodology, J.G.N.E., A.E.M., C.D., A.I. and T.K.; validation, C.D. and A.I.; formal analysis, A.E.M. and T.K.; investigation, J.G.N.E. and A.E.M.; data curation, J.G.N.E. and A.E.M.; writing—original draft preparation, J.G.N.E.; writing—review and editing, J.G.N.E., A.E.M., C.D., A.I., T.K. and J.P.; supervision, C.D.; project administration, C.D.; funding acquisition, C.D. All authors have read and agreed to the published version of the manuscript.

Funding: This research received no external funding.

Institutional Review Board Statement: Not applicable.

Informed Consent Statement: Not applicable.

Data Availability Statement: The data that support the findings of this study are available from the corresponding author, upon reasonable request.

Acknowledgments: The authors would like to thank the Nord-Pas de Calais Regional Council for financing this study. We are also grateful to the ASBois (Saint-Floris, France), Biallais Ind. (Saint-Augustin, France) and Holcim (Lumbres, France) companies for their support throughout this research project.

Conflicts of Interest: The authors declare no conflict of interest. The funders had no role in the design of the study; in the collection, analyses, or interpretation of data; in the writing of the manuscript, or in the decision to publish the results.

References

- Faruk, O.; Bledzki, A.K.; Fink, H.-P.; Sain, M. Biocomposites reinforced with natural fibers: 2000–2010. *Prog. Polym. Sci.* **2012**, *37*, 1552–1596. [\[CrossRef\]](#)
- Gholampour, A.; Ozbakkaloglu, T. A review of natural fiber composites: Properties, modification and processing techniques, characterization, applications. *J. Mater. Sci.* **2020**, *55*, 829–892. [\[CrossRef\]](#)
- Onuaguluchi, O.; Banthia, N. Plant-based natural fibre reinforced cement composites: A review. *Cem. Concr. Compos.* **2016**, *68*, 96–108. [\[CrossRef\]](#)
- John, M.J.; Thomas, S. Biofibres and biocomposites. *Carbohydr. Polym.* **2008**, *71*, 343–364. [\[CrossRef\]](#)
- Pacheco-Torgal, F.; Jalali, S. Cementitious building materials reinforced with vegetable fibres: A review. *Constr. Build. Mater.* **2011**, *25*, 575–581. [\[CrossRef\]](#)
- Bui, T.T.H.; Boutouil, M.; Sebaibi, N.; Levacher, D. Effect of Coconut Fiber Content on the Mechanical Properties of Mortars. *Acad. J. Civ. Eng.* **2019**, *37*, 300–307. [\[CrossRef\]](#)
- Agopyan, V.; Savastano, H.; John, V.; Cincotto, M. Developments on vegetable fibre–cement based materials in São Paulo, Brazil: An overview. *Cem. Concr. Compos.* **2005**, *27*, 527–536. [\[CrossRef\]](#)
- Silva, F.D.A.; Filho, R.D.T.; Filho, J.D.A.M.; Fairbairn, E.D.M.R. Physical and mechanical properties of durable sisal fiber–cement composites. *Constr. Build. Mater.* **2010**, *24*, 777–785. [\[CrossRef\]](#)
- Savastano, H.J.; Turner, A.; Mercer, C.; Soboyejo, W.O. Mechanical behavior of cement-based materials reinforced with sisal fibers. *J. Mater. Sci.* **2006**, *41*, 6938–6948. [\[CrossRef\]](#)
- Tonoli, G.; Savastano, H., Jr.; Fuente, E.; Negro, C.; Blanco, A.; Lahr, F.R. Eucalyptus pulp fibres as alternative reinforcement to engineered cement-based composites. *Ind. Crop. Prod.* **2010**, *31*, 225–232. [\[CrossRef\]](#)
- Sudin, R.; Swamy, N. Bamboo and wood fibre cement composites for sustainable infrastructure regeneration. *J. Mater. Sci.* **2006**, *41*, 6917–6924. [\[CrossRef\]](#)
- Chabannes, M.; Bénézet, J.-C.; Clerc, L.; Garcia-Diaz, E. Use of raw rice husk as natural aggregate in a lightweight insulating concrete: An innovative application. *Constr. Build. Mater.* **2014**, *70*, 428–438. [\[CrossRef\]](#)
- Savastano, H.; Agopyan, V. Transition zone studies of vegetable fibre–cement paste composites. *Cem. Concr. Compos.* **1999**, *21*, 49–57. [\[CrossRef\]](#)
- Page, J.; Sonebi, M.; Amziane, S. Design and multi-physical properties of a new hybrid hemp-flax composite material. *Constr. Build. Mater.* **2017**, *139*, 502–512. [\[CrossRef\]](#)
- Page, J.; Djelal, C.; Vanhove, Y. Optimisation of vibrocompaction process for wood-based concrete blocks. *Int. J. Adv. Manuf. Technol.* **2020**, *109*, 1189–1204. [\[CrossRef\]](#)
- Momoh, E.O.; Osofero, A.I. Recent developments in the application of oil palm fibers in cement composites. *Front. Struct. Civ. Eng.* **2020**, *14*, 94–108. [\[CrossRef\]](#)
- Bilba, K.; Arsene, M.-A.; Ouensanga, A. Sugar cane bagasse fibre reinforced cement composites. Part I. Influence of the botanical components of bagasse on the setting of bagasse/cement composite. *Cem. Concr. Compos.* **2003**, *25*, 91–96. [\[CrossRef\]](#)
- Page, J.; Amziane, S.; Gomina, M.; Djelal, C.; Audonnet, F. Using linseed oil as flax fibre coating for fibre-reinforced cementitious composite. *Ind. Crop. Prod.* **2021**, *161*, 113168. [\[CrossRef\]](#)
- Magniont, C.; Escadeillas, G. Chemical Composition of Bio-Aggregates and Their Interactions with Mineral Binders. In *Bio-aggregates Based Building Materials: State-of-the-Art Report of the RILEM Technical Committee 236-BBM*; RILEM State-of-the-Art Reports; Amziane, S., Collet, F., Eds.; Springer: Dordrecht, The Netherlands, 2017; pp. 1–37. ISBN 978-94-024-1031-0.
- Page, J.; Khadraoui, F.; Gomina, M.; Boutouil, M. Hydration of flax fibre-reinforced cementitious composites: Influence of fibre surface treatments. *Eur. J. Environ. Civ. Eng.* **2021**, 1–23. [\[CrossRef\]](#)
- Wei, Y.M.; Tomita, B.; Hiramatsu, Y.; Miyatake, A.; Fujii, T. Study of hydration behaviors of wood–cement mixtures: Compatibility of cement mixed with wood fiber strand obtained by the water-vapor explosion process. *J. Wood Sci.* **2002**, *48*, 365–373. [\[CrossRef\]](#)
- Govin, A.; Peschard, A.; Guyonnet, R. Modification of cement hydration at early ages by natural and heated wood. *Cem. Concr. Compos.* **2006**, *28*, 12–20. [\[CrossRef\]](#)

23. Page, J.; Khadraoui, F.; Gomina, M.; Boutouil, M. Influence of different surface treatments on the water absorption capacity of flax fibres: Rheology of fresh reinforced-mortars and mechanical properties in the hardened state. *Constr. Build. Mater.* **2019**, *199*, 424–434. [\[CrossRef\]](#)
24. Ramakrishna, G.; Sundararajan, T. Impact strength of a few natural fibre reinforced cement mortar slabs: A comparative study. *Cem. Concr. Compos.* **2005**, *27*, 547–553. [\[CrossRef\]](#)
25. Collet, F.; Pretot, S. Thermal conductivity of hemp concretes: Variation with formulation, density and water content. *Constr. Build. Mater.* **2014**, *65*, 612–619. [\[CrossRef\]](#)
26. Glé, P.; Gourdon, E.; Arnaud, L. Acoustical properties of materials made of vegetable particles with several scales of porosity. *Appl. Acoust.* **2011**, *72*, 249–259. [\[CrossRef\]](#)
27. Grubeša, I.N.; Marković, B.; Gojević, A.; Brdarić, J. Effect of hemp fibers on fire resistance of concrete. *Constr. Build. Mater.* **2018**, *184*, 473–484. [\[CrossRef\]](#)
28. Lo, T.Y.; Tang, W.; Cui, H. The effects of aggregate properties on lightweight concrete. *Build. Environ.* **2007**, *42*, 3025–3029. [\[CrossRef\]](#)
29. Delannoy, G.; Marceau, S.; Glé, P.; Gourlay, E.; Guéguen-Minerbe, M.; Amziane, S.; Farcas, F. Durability of hemp concretes exposed to accelerated environmental aging. *Constr. Build. Mater.* **2020**, *252*, 119043. [\[CrossRef\]](#)
30. Filho, R.D.T.; Scrivener, K.; England, G.L.; Ghavami, K. Durability of alkali-sensitive sisal and coconut fibres in cement mortar composites. *Cem. Concr. Compos.* **2000**, *22*, 127–143. [\[CrossRef\]](#)
31. Filho, R.D.T.; Ghavami, K.; England, G.L.; Scrivener, K. Development of vegetable fibre-mortar composites of improved durability. *Cem. Concr. Compos.* **2003**, *25*, 185–196. [\[CrossRef\]](#)
32. Hosseinpourpia, R.; Varshoe, A.; Soltani, M.; Hosseini, P.; Tabari, H.Z. Production of waste bio-fiber cement-based composites reinforced with nano-SiO₂ particles as a substitute for asbestos cement composites. *Constr. Build. Mater.* **2012**, *31*, 105–111. [\[CrossRef\]](#)
33. Hosseini, P.; Booshehrian, A.; Farshchi, S. Influence of Nano-SiO₂ Addition on Microstructure and Mechanical Properties of Cement Mortars for Ferrocement. *Transp. Res. Rec. J. Transp. Res. Board* **2010**, *2141*, 15–20. [\[CrossRef\]](#)
34. Aigbomian, E.P.; Fan, M. Development of Wood-Crete building materials from sawdust and waste paper. *Constr. Build. Mater.* **2012**, *40*, 361–366. [\[CrossRef\]](#)
35. Sales, A.; de Souza, F.R.; Almeida, F.C. Mechanical properties of concrete produced with a composite of water treatment sludge and sawdust. *Constr. Build. Mater.* **2011**, *25*, 2793–2798. [\[CrossRef\]](#)
36. Engone, J.G.N.; Vanhove, Y.; Djelal, C.; Kada, H. Optimizing mortar extrusion using poplar wood sawdust for masonry building block. *Int. J. Adv. Manuf. Technol.* **2018**, *95*, 3769–3780. [\[CrossRef\]](#)
37. Belhadji, B.; Bederina, M.; Montrelay, N.; Houessou, J.; Quéneudec, M. Effect of substitution of wood shavings by barley straws on the physico-mechanical properties of lightweight sand concrete. *Constr. Build. Mater.* **2014**, *66*, 247–258. [\[CrossRef\]](#)
38. Mohammed, B.S.; Abdullahi, M.; Hoong, C. Statistical models for concrete containing wood chipping as partial replacement to fine aggregate. *Constr. Build. Mater.* **2014**, *55*, 13–19. [\[CrossRef\]](#)
39. Berra, M.; Mangialardi, T.; Paolini, A.E. Reuse of woody biomass fly ash in cement-based materials. *Constr. Build. Mater.* **2015**, *76*, 286–296. [\[CrossRef\]](#)
40. Udoeyo, F.F.; Inyang, H.; Young, D.T.; Oparadu, E.E. Potential of Wood Waste Ash as an Additive in Concrete. *J. Mater. Civ. Eng.* **2006**, *18*, 605–611. [\[CrossRef\]](#)
41. Yasuda, S.; Ima, K.; Matsushita, Y. Manufacture of wood-cement boards VII: Cement-hardening inhibitory compounds of hannoki (Japanese alder, *Alnus japonica* Steud.). *J. Wood Sci.* **2002**, *48*, 242–244. [\[CrossRef\]](#)
42. Papadopoulos, A.N. An investigation of the suitability of some Greek wood species in wood-cement composites manufacture. *Holz Roh Werkst.* **2007**, *65*, 245–246. [\[CrossRef\]](#)
43. Oyagade, A.O. Effect of Cement/Wood Ratio on the Relationship between Cement Bonded Particleboard Density and Bending Properties. *J. Trop. For. Sci.* **1990**, *2*, 211–219.
44. Okino, E.Y.; de Souza, M.R.; Santana, M.A.; Alves, M.V.S.; de Sousa, M.E.; Teixeira, D.E. Physico-mechanical properties and decay resistance of *Cupressus* spp. cement-bonded particleboards. *Cem. Concr. Compos.* **2005**, *27*, 333–338. [\[CrossRef\]](#)
45. Beltran, M.S.; Schlangen, E. Wood Fibre Reinforced Cement Matrix: A Micromechanical Based Approach. *Key Eng. Mater.* **2008**, *385–387*, 445–448. [\[CrossRef\]](#)
46. Djelal, C.; Page, J.; Kada, H.; Vanhove, Y. Feasibility study of using poplar wastes as sand in cement mortars. *J. Mater. Cycles Waste Manag.* **2020**, *22*, 488–500. [\[CrossRef\]](#)
47. Bentur, A. *Fibre Reinforced Cementitious Composites*, 2nd ed.; Modern Concrete Technology Series; Taylor & Francis: London, UK; New York, NY, USA, 2007; ISBN 978-0-415-25048-1.
48. Wei, Y.M.; Zhou, Y.G.; Tomita, B. Hydration behavior of wood cement-based composite I: Evaluation of wood species effects on compatibility and strength with ordinary portland cement. *J. Wood Sci.* **2000**, *46*, 296–302. [\[CrossRef\]](#)
49. Fan, M.; Ndikontar, M.K.; Zhou, X.; Ngamveng, J.N. Cement-bonded composites made from tropical woods: Compatibility of wood and cement. *Constr. Build. Mater.* **2012**, *36*, 135–140. [\[CrossRef\]](#)
50. Mouhmid, B.; Imad, A.; Benseddik, N.; Benmedakhène, S.; Maazouz, A. A study of the mechanical behaviour of a glass fibre reinforced polyamide 6,6: Experimental investigation. *Polym. Test.* **2006**, *25*, 544–552. [\[CrossRef\]](#)

51. Voigt, W. Ueber die Beziehung zwischen den beiden Elasticitätsconstanten isotroper Körper. *Ann. Phys.* **1889**, *274*, 573–587. [[CrossRef](#)]
52. Reuss, A. Berechnung der Fließgrenze von Mischkristallen auf Grund der Plastizitätsbedingung für Einkristalle. *Z. Angew. Math. Mech.* **1929**, *9*, 49–58. [[CrossRef](#)]
53. Hashin, Z.; Shtrikman, S. A variational approach to the theory of the elastic behaviour of multiphase materials. *J. Mech. Phys. Solids* **1963**, *11*, 127–140. [[CrossRef](#)]
54. Mori, T.; Tanaka, K. Average stress in matrix and average elastic energy of materials with misfitting inclusions. *Acta Met.* **1973**, *21*, 571–574. [[CrossRef](#)]
55. Bary, B.; Ben Haha, M.; Adam, E.; Montarnal, P. Numerical and analytical effective elastic properties of degraded cement pastes. *Cem. Concr. Res.* **2009**, *39*, 902–912. [[CrossRef](#)]
56. Bentz, D.P. Three-Dimensional Computer Simulation of Portland Cement Hydration and Microstructure Development. *J. Am. Ceram. Soc.* **1997**, *80*, 3–21. [[CrossRef](#)]
57. Béjaoui, S.; Bary, B.; Nitsche, S.; Chaudanson, D.; Blanc, C. Experimental and modeling studies of the link between microstructure and effective diffusivity of cement pastes. *Rev. Eur. Génie Civ.* **2006**, *10*, 1073–1106. [[CrossRef](#)]
58. Bishnoi, S.; Scrivener, K.L. μic : A new platform for modelling the hydration of cements. *Cem. Concr. Res.* **2009**, *39*, 266–274. [[CrossRef](#)]
59. Nagai, G.; Yamada, T.; Wada, A. Stress Analysis of Concrete Material Based on Geometrically Accurate Finite Element Modeling. In *Proceedings of FRAMCOS-3*; AEDIFICATIO Publishers: Freiburg, Germany, 1998; pp. 1077–1086.
60. Wriggers, P.; Moftah, S. Mesoscale models for concrete: Homogenisation and damage behaviour. *Finite Elements Anal. Des.* **2006**, *42*, 623–636. [[CrossRef](#)]
61. Caballero, A.; López, C.; Carol, I. 3D meso-structural analysis of concrete specimens under uniaxial tension. *Comput. Methods Appl. Mech. Eng.* **2006**, *195*, 7182–7195. [[CrossRef](#)]
62. Escoda, J.; Jeulin, D.; Willot, F.; Toulemonde, C. Three-dimensional morphological modelling of concrete using multiscale Poisson polyhedra. *J. Microsc.* **2015**, *258*, 31–48. [[CrossRef](#)]
63. He, H.; Guo, Z.; Stroeven, P.; Stroeven, M.; Sluys, L.J. Strategy on Simulation of Arbitrary-Shaped Cement Grains in Concrete. *Image Anal. Ster.* **2011**, *29*, 79–84. [[CrossRef](#)]
64. El Moumen, A.; Kanit, T.; Imad, A.; Minor, H.E. Effect of overlapping inclusions on effective elastic properties of composites. *Mech. Res. Commun.* **2013**, *53*, 24–30. [[CrossRef](#)]
65. EL Moumen, A.; Kanit, T.; Imad, A.; El Minor, H. Effect of reinforcement shape on physical properties and representative volume element of particles-reinforced composites: Statistical and numerical approaches. *Mech. Mater.* **2015**, *83*, 1–16. [[CrossRef](#)]
66. Lippmann, N.; Steinkopff, T.; Schmauder, S.; Gumbsch, P. 3D-finite-element-modelling of microstructures with the method of multiphase elements. *Comput. Mater. Sci.* **1997**, *9*, 28–35. [[CrossRef](#)]